JℲM PAPERS

Dynamics of directional soluble wicking

Sohyun Jung[1], Wonjung Kim[2],† and Ho-Young Kim[1],†

[1]Department of Mechanical Engineering, Seoul National University, Seoul 08826, Korea

[2]Department of Mechanical Engineering, Sogang University, Seoul 04107, Korea

Liquids can invade fibrous porous media when the fibres are either wettable or soluble, and the infiltration rate can differ depending on spatial distribution of fibres as well as liquid properties. With continuing developments in dissolution-driven release mechanisms of porous drugs and chemical pattern formations, the understanding of how liquids spontaneously infiltrate into soluble fibrous media is strongly called for. Here we show that unlike capillarity-driven insoluble wicking (exhibiting diffusive growth of wetting distance with time), the wicking distance in soluble porous media grows linearly with time as dominated by liquid viscosity rather than surface tension. Such soluble wicking is highly sensitive to flow orientation relative to fibre alignment, so that it arises only in the crosswise direction while being strongly inhibited in the lengthwise direction. We present a theoretical model to explain the experimentally measured wicking rates in soluble porous media.

Key words: capillary flows, porous media, microfluidics

1. Introduction

Liquid flows infiltrating into porous media are found in a variety of situations, including painting (Kim *et al.* 2015) and writing (Kim *et al.* 2011) on paper, wetting of soils (Raux *et al.* 2013) and hydrogels (Yoon *et al.* 2010) and absorption in hygiene items (Landeryou, Eames & Cottenden 2005). When the media are wettable but insoluble in the liquid, the flow velocity is determined by the balance of capillary driving force and viscous resisting force. A simple approach considering the voids as an assemblage of cylindrical conduits predicts that the wetting distance will grow like $t^{1/2}$ with t being time (Washburn 1921), which has been widely adopted to explain basic wetting dynamics of porous media for over a century. However, variations of the wetting dynamics can arise as a result of a number of factors, such as effects of gravity (Kim, Ha & Kim 2017), poroelastic response

† Email addresses for correspondence: wonjungkim@sogang.ac.kr, hyk@snu.ac.kr

of soft solids (Ha *et al.* 2018), spatial irregularities or directionality of pore networks (Xia & Brueck 2008) and solubility of medium solids (Twist & Zatz 1988).

In particular, liquid invasion in soluble porous media plays an essential role in drug delivery, where porous drugs should be dissolved to release their contents at a controlled rate where and when desirable. Liquid flows caused by pressurized injection, rather than spontaneous capillary imbibition, and subsequent dissolution in soluble porous media were previously investigated with a major focus on the formation of ramified patterns (Daccord 1987; Szymczak & Ladd 2011). In drug delivery, the role of porosity in drug release rate was experimentally studied when the governing step of drug response was swelling (Colombo *et al.* 1996) or dissolution (Brielles *et al.* 2007). Despite these pioneering but limited studies, the fundamental physical understanding of capillarity-driven imbibition dynamics coupled with dissolution in drug delivery has rarely been attempted and as a result is still far from complete.

Here, we study the capillarity-assisted invasion of liquid in porous media, referred to as wicking, the dynamics of which changes sensitively with directionality of the porous network as well as the solubility of the solid. As a model system to study the dynamics of directional soluble wicking, we use porous sheets of polyethylene oxide (PEO) fibres. By controlling the ordering of fibres in the fibre deposition process, we can investigate the effects of fibre directionality (random or directional) on the preferred orientation and rates of wicking dynamics. Polyethylene oxide can be dissolved in aqueous solutions, but is insoluble in ethylene glycol and silicone oil. Thus, we can compare the imbibition dynamics of dissolving and non-dissolving liquids to find the effects of dissolution on the rates of wicking dynamics. We find that the rate of soluble wicking is determined by a completely different process from that of insoluble wicking, thereby giving different power laws of wicking distance. Furthermore, such effects of dissolution are shown to give rise to a counterintuitive wicking behaviour in soluble sheets of aligned fibres, so that wicking occurs dominantly in the crosswise, rather than the lengthwise, direction.

In the following, we start with an explanation of the experimental processes for fabricating porous sheets of fibres and for observing the wicking dynamics. We then briefly review basic theories associated with capillarity-driven non-reactive liquid flows in porous media. We list our observation results of wicking flows, where the basic wicking dynamics in insoluble porous sheets of randomly deposited fibres serves as a basis to identify the effects of fibre alignment and solubility. We theoretically analyse the wicking rates by identifying essential physics governing the flows, which yields power laws consistent with experimental data.

2. Materials and methods

For porous substrates to imbibe liquids, we used sheets of fibres of PEO (Sigma Aldrich) with a molecular weight of 3×10^5, which were produced by electrospinning. A jet of aqueous PEO solution of 10 wt% concentration was ejected from a metal capillary of 0.26 mm in inner diameter under an electric field of $100 \, kV \, m^{-1}$. The jet was partially solidified during flight and deposited on a collector as fibres. On a flat plate ground, the fibres were chaotically deposited as shown in figure 1(*a*) to yield a sheet of average thickness of 77 μm. The fibres were aligned in one direction on the surface of a drum collector rotating at the same linear speed as the jet ($4.7 \, m \, s^{-1}$) (Shin *et al.* 2018), as shown in figure 1(*b*). The average thickness of the sheets obtained by the directional electrospinning process was 33 μm. In the image, we find some fibres crossing the uniformly aligned fibres, which play an important role in guide wicking in some cases as discussed below. The average
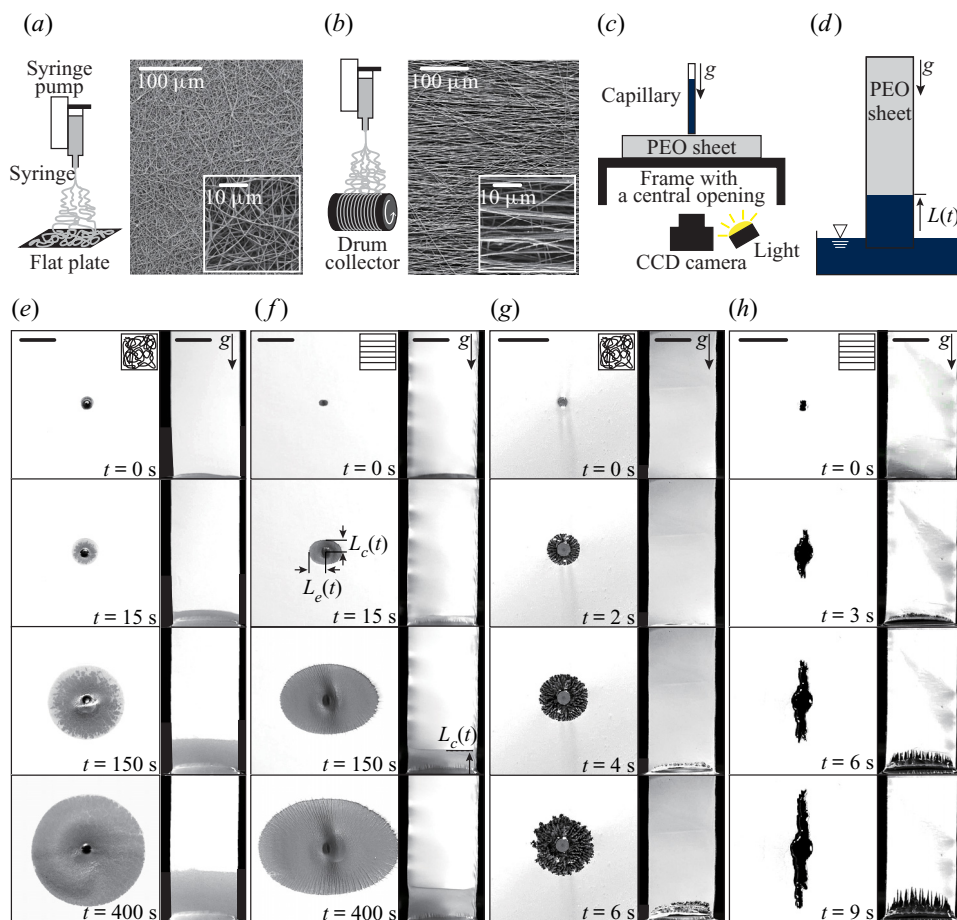
Figure 1. (*a*) Random deposition of electrospun fibres of PEO, and the corresponding SEM image. (*b*) Directional deposition of electrospun fibres of PEO, and the corresponding SEM image. (*c*) Wicking of a liquid from a point source emanating from a capillary tube touching a PEO fibrous sheet. (*d*) Propagation of liquid front against gravity into a strip of fibrous PEO sheet. (*e*) Wicking of ethylene glycol in a randomly deposited insoluble sheet. (*f*) Wicking of ethylene glycol in a directionally deposited insoluble sheet. (*g*) Wicking of water in a randomly deposited soluble sheet. (*h*) Wicking of water in a directionally deposited soluble sheet. In (*e–h*), the left and right columns correspond to the flows from a point source (capillary) and a liquid pool, respectively. Small boxes in the top row of (*e–h*) indicate fibre alignment. Scale bars, 5 mm.

radius of fibres was measured using scanning electron microscopy (SEM) images, and the porosity was obtained by comparing the densities of PEO and the fibrous sheets. The characteristics of the fibrous sheets are listed in table 1. The average distance between aligned fibres in the directionally electrospun substrates was measured via SEM images to be 7 µm with a standard deviation of 3 µm.

The liquids used in our experiments are ethylene glycol, silicone oil, water, aqueous ethylene glycol of various concentrations and chloroform, the physical properties of which are listed in table 2. Liquids *A* and *B* have a contact angle of nearly zero with PEO sheets but do not dissolve the fibres. The other liquids (*C* to *F*) dissolve PEO. We observed wicking of a liquid emanating from a capillary tube on a porous substrate due to capillary action to check the directionality of the spreading dynamics, as shown in figure 1(*c*). The rate of one-dimensional wicking was separately measured by observing the propagation of

Sheet	Random	Directional
Fibre radius, R_f, $\pm$ std (nm)	209 ± 38	234 ± 50
Porosity, ϕ	0.84	0.65
Equivalent pore radius, R (μm)	2.3	0.86
Permeability, k, measured (m^2)	4.8×10^{-14}	4.1×10^{-15}
Permeability, k, modelled (m^2)	4.8×10^{-14}	4.4×10^{-15}

Table 1. Characteristics of the porous fibrous sheets. For fibre radius, std stands for standard deviation.

	Liquid	Surface tension (mN m^{-1})	Viscosity (mPa s)	Density (kg m^{-3})	Symbol Random	Symbol Directional ($\perp$, $\parallel$)
A	Ethylene glycol (EG)	47	21.1	1112	◑	○,●
B	Silicone oil	40	10.0	939	◆	◇,◆
C	Water	72	1	997	▲	△,▲
D	Aqueous EG (10 wt%)	67	1.4	1042	▶	▷,▶
E	Aqueous EG (20 wt%)	59	1.9	1068	◀	◁,◀
F	Chloroform	27	0.6	1490	▼	▽,▼

Table 2. Properties of liquids used in the experiments at a temperature of 25 °C. Symbols are also listed that appear in figures 3–6 indicating the experimental conditions. Symbols $\perp$ and $\parallel$ indicate crosswise and lengthwise wicking, respectively.

the wetting front, $L(t)$, in a 1 cm wide strip from the free surface of a liquid pool, as shown in figure 1(*d*).

The deformation of PEO fibres in response to humidity change was visualized using an environmental SEM (ESEM) instrument (Philips XL-30 FEG). We placed a fibrous PEO sheet measuring 5 mm × 5 mm in area on a Peltier plate whose surface temperature was kept at 2 °C. The relative humidity in the ESEM chamber was varied from 25 % to 95 % during experiments.

3. Fundamental theories of capillary flows in porous media

Here, we briefly review the fundamental theories of capillary flows in porous media, on which our theoretical development will be based. Most porous media are of great complexity, so theoretical attempts to understand the dynamics of liquids in porous media have been made through the conceptual model approach (Scheidegger 1960). The simplest model representing a porous medium is a bundle of straight, parallel capillaries of uniform diameter. Using this model, we first consider the velocity of the liquid front in a wettable capillary of radius R, as shown in figure 2(*a*). The average velocity of incompressible liquid flow u in a small axisymmetric straight capillary of radius R ($R \ll L$) follows the Poiseuille law written as $u = R^2(-\mathrm{d}p/\mathrm{d}x)/(8\mu)$, with L, μ and p, respectively, being the propagation distance of the liquid, the viscosity and the pressure. For inertialess surface-tension-driven flow neglecting gravity, the pressure difference is $\Delta p = p_a - p_i$, where p_a is the atmospheric pressure and p_i is the internal pressure at the liquid–gas interface. As the pressure of air just outside of the liquid–gas interface is also
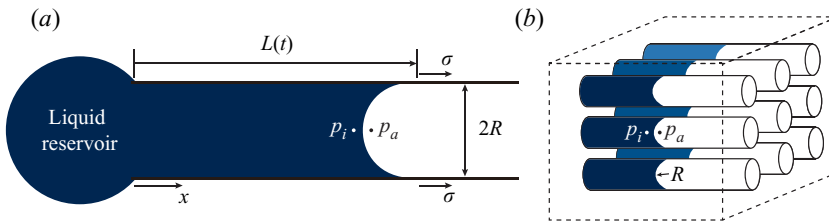
Figure 2. (*a*) A schematic of liquid imbibition into a capillary with a contact angle of zero under negligible effects of gravity. (*b*) A schematic of liquid imbibition into a porous medium.

p_a, we realize that Δp is equal to the pressure jump across the interface, which is given by the Laplace–Young equation, $\Delta p = \sigma \kappa$, with κ being the interface curvature (de Gennes, Brochard-Wyart & Quéré 2004). In a wettable capillary, $\kappa \approx 2R^{-1}$, and thus the average fluid velocity becomes $u = \sigma R/(4\mu L)$. Using $u = \dot{L}$, we obtain the classical diffusive behaviour of the wetted length with time t: $L = [\sigma R t/(2\mu)]^{1/2}$ (Lucas 1918; Washburn 1921).

We now turn to fluid flows in porous media, as shown in figure 2(*b*), modelled as a bundle of capillaries having the same radius R, embedded in a solid. If N tubes are embedded in the unit cross-sectional area, then the total flow rate per unit cross-sectional area, q_m, is $N\pi R^2 u$. Thus, we have $q_m = \phi R^2(-\mathrm{d}p/\mathrm{d}x)/(8\mu)$, where the porosity ϕ (the fraction of the volume of voids over the total volume) is $N\pi R^2$.

The fluid flow in porous media with negligible inertia is described by Darcy's law (Darcy 1856; Bear 1972). For one-dimensional fluid flow, Darcy's law is written as $q_t = k/\mu(-\mathrm{d}p/\mathrm{d}x)$, which corresponds to the linear relationship between the total flow rate per unit area q_t and the pressure gradient, with k/μ being the prefactor. Here, k is the permeability. The analogy between q_m and Darcy's law is obvious. In q_m, $\phi R^2/8$ is analogous to the permeability k. In applying this relationship to an actual porous medium, R scales as an average pore radius.

The permeability k is highly related to the geometrical properties of pores, such as porosity, average size, size distribution and shape. Although the relationship between geometrical pore characteristics and permeability has long been under discussion through empirical (Nelson & Baver 1940; Jacob 1946; Baver 1949; Griffiths 1952) and theoretical (Kozeny 1927; Carman 1941; Purcell 1949; Cornell & Katz 1953; Rose & Witherspoon 1956) studies, these attempts have only found the empirical relations for average permeability of porous media due to the complex nature of pore structure. Still, it is reasonable to scale the permeability as the cross-sectional area of actual fluid conduits.

4. Results and discussion

4.1. *Types of wicking dynamics*

Depending on the solubility in liquid and the directionality of fibres constituting the substrate, we obtain four different categories of experimental conditions to determine the wicking dynamics.

(i) When the fibres are randomly deposited and insoluble in the liquid, the wicking occurs independent of direction exhibiting a circular wet area growing from a point source as shown in the left-hand column of figure 1(*e*). For the insoluble strip contacting a free surface of the liquid, a horizontal wetting front advances against the direction of gravity as shown in the right-hand column of figure 1(*e*).

(ii) When the fibres are aligned and insoluble, the liquid wicks faster along the fibre direction than across the direction. Thus, the wet area growing from a point source is elliptical with the major axis coinciding with the fibre alignment direction, as shown in the left-hand column of figure 1(*f*). A relatively smooth horizontal wetting front propagates from a free surface as shown in the right-hand column of figure 1(*f*) with the speeds different depending on the orientation of fibres relative to a free surface of liquid.

(iii) When the fibres are randomly deposited but soluble in the liquid, the wicking tends to occur independent of direction with spiky circular fronts from a point source as shown in the left-hand column of figure 1(*g*). The rough horizontal wetting front advances from a free surface as shown in the right-hand column of figure 1(*g*).

(iv) When the fibres are aligned but soluble, the liquid wicks much faster in the crosswise direction than the lengthwise direction. Thus, the wet area growing from a point source elongates in a direction perpendicular to aligned fibres while the wicking along the fibres is severely suppressed as shown in the left-hand column of figure 1(*h*). The wetting front advancing from a liquid pool's free surface is fairly spiky when the free surface and the fibre directions are parallel, as shown in the right-hand column of figure 1(*h*). Wicking was hardly observed when the strip touched the free surface with the fibre direction perpendicular to the free surface.

4.2. *Insoluble wicking*

We start with the dynamics of wicking of liquids in insoluble fibrous sheets, representative images of which are shown in figure 1(*e*,*f*). We first consider the wicking rates of liquids in the sheets of randomly deposited fibres. As delineated in § 3, in porous media with homogeneous porosity, one-dimensional fluid flows follow Darcy's law: $q = k_r \Delta p/(\mu L_r)$, where q, k_r and L_r are, respectively, the average fluid velocity over the unit area, the permeability and the wicking distance. However, the flow velocity that we observe is the average local fluid flow velocity u, which must be greater than the average fluid velocity over the unit area owing to the solid area in porous media. According to the commonly accepted hypothesis known as the Dupuit–Forchheimer assumption (Dupuit 1863; Forchheimer 1986), the average local fluid flow velocity u is q/ϕ, which leads to $u = k_r \Delta p/(\phi \mu L_r)$. If capillarity drives the flow in the wettable media with negligible gravitational effects owing to a very low Bond number, $Bo = \rho g R^2/\sigma \sim O(10^{-6})$, the pressure difference established between the reservoir and the interior of advancing meniscus is equal to the Laplace pressure, $\Delta p = 2\sigma/R$, where R, ρ and g are the equivalent pore radius, liquid density and gravitational acceleration, respectively. Modelling the porous sheet structure as a regular array of cylindrical conduits with equivalent hydraulic radius R, we estimate R using two measurable parameters, porosity ϕ and fibre radius R_f, as $R = R_f \phi/(1 - \phi)$ (Mao & Russell 2008). Then, taking $q = \dot{L}_r$ in Darcy's law and integrating with respect to time from $t = 0$ to t gives

$$L_r = 2 \left[\frac{(1 - \phi)k_r}{\phi^2 R_f} \frac{\sigma}{\mu} \right]^{1/2} t^{1/2}. \tag{4.1}$$

We plot the wicking distance of liquids A and B in the sheets of randomly deposited fibres in figure 3(*a*). Although the wicking occurs at different rates for the differing properties of the liquids (inset in the figure), the measurement data of wicking distance are collapsed onto a single line when plotted according to (4.1). The diffusive behaviour of the wetting distance on two-dimensionally isotropic insoluble porous sheets is consistent with results of prior studies using fibrous sheets of non-woven fabrics (Kim *et al.* 2015) and
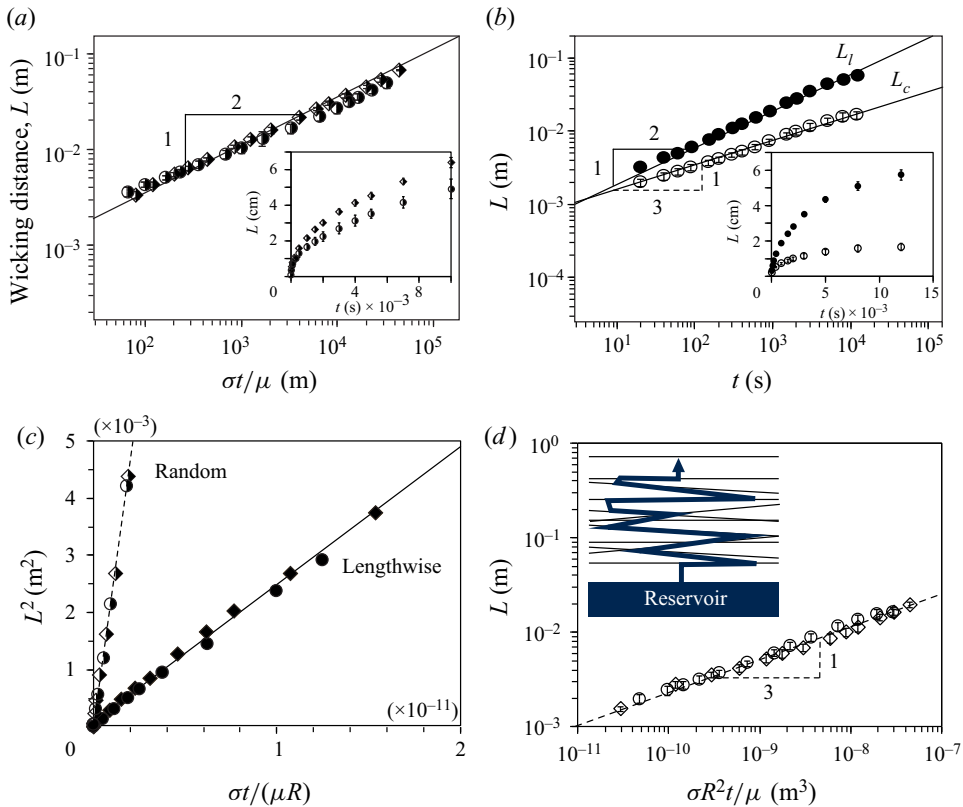
Figure 3. (*a*) The wicking distance of liquids *A* and *B* in insoluble porous sheets of randomly deposited fibres plotted according to (4.1). Inset: raw data of *L* versus *t*. (*b*) The wicking distance of liquid *A* in insoluble sheets of directionally deposited fibres. Different power laws are observed depending on the flow direction. Inset: linear plots of L_l and L_c versus *t*. (*c*) The wicking distances in insoluble sheets of randomly deposited fibres, and the lengthwise wicking distances in insoluble sheets of directionally deposited fibres, plotted according to scaling law (4.1). The slopes of the best-fitting lines corresponding to $4k_r/\phi$ are 2.3×10^{-13} and 2.5×10^{-14} m^2 for random and directional substrates, respectively. (*d*) The crosswise wicking distance of liquids *A* and *B* plotted versus $\sigma R t/\mu$.

paper (Kim *et al.* 2011). The slope of the best-fitting dotted line in figure 3(*c*) corresponds to $4k_r/\phi$, and we find the permeability of the insoluble porous sheet of randomly deposited fibres to be $k_r = 4.8 \times 10^{-14}$ m^2.

We now consider the wicking rates in the sheets of directionally deposited fibres as shown in figure 1(*f*). As the wicking rate depends on the direction of flow relative to fibre alignment, we plot the temporal evolutions of the lengthwise imbibition L_l and the crosswise imbibition L_c in figure 3(*b*). We see different power laws observed depending on the wicking direction, so that $L_l \sim t^{1/2}$ and $L_c \sim t^{1/3}$. The diffusive behaviour of L_l indicates that the lengthwise flow follows Darcy's law as driven by capillarity. Thus, we express L_l in the same form as (4.1), $L_l = 2[(1 - \phi)k_l\sigma/(\phi^2 R_f\mu)]^{1/2}t^{1/2}$, with k_l being the permeability of the directionally deposited sheet, which collapses the raw data of L_l of liquids *A* and *B* onto a single line, as shown in figure 3(*c*). The slope of the line of best fit empirically gives the permeability, $k_l = 4.1 \times 10^{-15}$ m^2.

Given the measured values of permeability in random and directional fibrous sheets, we check whether they can be predicted by a previous model (Rodriguez, Giacomelli &

Vazquez 2004) which proposes the following form of k as a function of porosity: $k = \phi^{n+1}(1 - \phi)^{-n}/C$, where n and C are empirical parameters. Taking $n = 0.97$, a value corresponding to fibreglass in Rodriguez *et al.* (2004), we find $C = 2.6 \times 10^{14}$ m^{-2} to match the measured and predicted permeabilities of a random deposited sheet, $k_r = 4.8 \times 10^{-14}$ m^2. The chosen values of n and C lead to the following value of the permeability in the directionally deposited sheet predicted: $k_l = 4.4 \times 10^{-15}$ m^2. This matches closely the measured value of $k_l = 4.1 \times 10^{-15}$ m^2. This is consistent with the previous finding (Rodriguez *et al.* 2004) that the permeability of porous media made of the same fibre materials exhibits the same functional dependency on porosity whether fibres are aligned or not.

For imbibition to arise in the crosswise direction, the liquid following the aligned fibres should either touch adjacent fibres upon bulging through the inter-fibre gaps (Bayramli & Powell 1990) or wick along misaligned fibres crossing the fibre alignments. Because the average inter-fibre distance (7 μm) is greater than the fibre radius (235 nm), the bulging is unlikely to convey liquid to adjacent fibres. Thus, the flow path for the crosswise impregnation is provided by occasionally encountered misaligned fibres, as schematically shown in the inset of figure 3(*d*). Since the pathway of crosswise wicking involves complex detours, the wicking dynamics no longer follows the classical diffusive rule.

With no theoretical models for the crosswise wicking available, we figure out the functional dependence of wicking distance on such independent parameters as t, R, σ and μ based on dimensional analysis (Buckingham 1914). The dimensionless crosswise wicking distance L_c/R is a function of a dimensionless time, $\sigma t/(\mu R)$. Assuming that a power law is observed, we write $L_c \sim (\sigma t/\mu)^{\alpha} R^{1-\alpha}$. We have seen above that $\alpha = 1/2$ for insoluble wicking in randomly deposited sheets and lengthwise imbibition in directional fibrous sheets. However, for crosswise wicking that suffers from infrequent but tortuous flow paths, α tends to decrease with an increase of the tortuosity, defined as the length ratio of the actual flow path to the straight path (Cai & Yu 2011). The tortuosity will increase as the number of misaligned fibres decreases. Upon finding that $L_c \sim t^{1/3}$ from our raw data, we have plotted L_c versus $\sigma R^2 t/\mu$ in figure 3(*d*), which validates that the power law is indeed observed with a power $\alpha = 1/3$ for the particular fibrous sheets used in this work.

4.3. *Wicking in randomly deposited soluble sheets*

While the PEO fibres are insoluble in liquids A and B, they are soluble in aqueous solutions (liquids C to E) and chloroform (liquid F). When liquids touch randomly deposited soluble porous sheets, the wicking rates are independent of direction although the wetting front is uneven. Figure 4(*a*) shows the soluble wicking dynamics qualitatively different from that in insoluble porous media, i.e. the wicking distance in soluble porous media grows linearly with time rather than increasing like $t^{1/2}$.

The transport of liquid in soluble porous media involves more complex processes than in insoluble porous media. In general, when polymer contacts its solvent, the polymer first swells by absorbing the solvent, and then turns into gel (a diluted cross-linked system with negligible fluidity). If the gel layer blocks flow paths in the fibrous network, the gel layer should be dissolved away into fresh solvent before liquid propagation resumes. To aid the understanding of soluble wicking dynamics in general, we consider two cases depending on the size of conduit relative to the degree of polymer swelling. First, the conduit is so large that the swelling of polymeric wall does not block the conduit but only modifies the capillary radius and the liquid properties (viscosity and surface tension), as illustrated in figure 5(*a*). Second, the conduit is so narrow that the polymer swelling
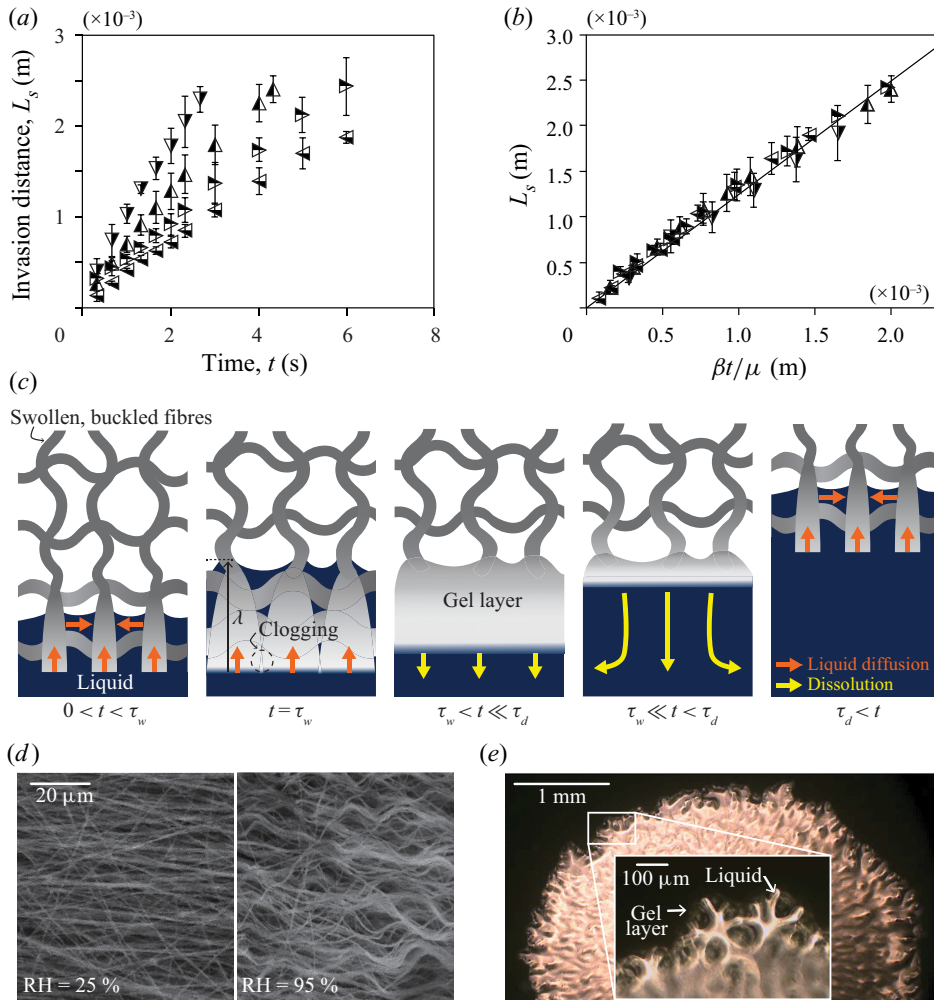
Figure 4. (*a*) The liquid invasion distance, L_s, of various liquids versus time in soluble porous sheets of randomly deposited PEO fibres. (*b*) Distance L_s versus $\beta t/\mu$, plotted according to scaling law (4.2). (*c*) Schematics of physical processes during wicking of a porous sheet of randomly deposited soluble fibres. The solvent diffuses in fibres (orange arrows), which swell and turn to a gel layer accordingly. The loosened polymer chains are dissolved away (yellow arrows) where they can meet fresh liquid, which becomes an instantaneously preferred direction of soluble wicking. (*d*) Two ESEM images of PEO fibres that swell and consequently buckle to contact with their neighbours under a high humidity (RH, relative humidity). (*e*) Inverted microscopy image of a soluble random porous sheet being impregnated by water, whose wet area appears bright.

blocks the channel rapidly as shown in figure 5(*b*). Wicking can resume only when the gel blocking the conduit is dissolved into the solvent.

In the first case, we need to consider simultaneous processes of longitudinal wicking and the polymer wall's transverse diffusion, swelling and dissolution. That is, as the wall swells, the capillary driving force and the viscous resistance change for the shrinking cross-section of fluid conduit. We also need to consider the loss of liquid for its transverse diffusion into the polymer wall and possible change of viscosity for polymer dissolution. This is a challenging problem that should couple capillary dynamics, kinetics of solvent
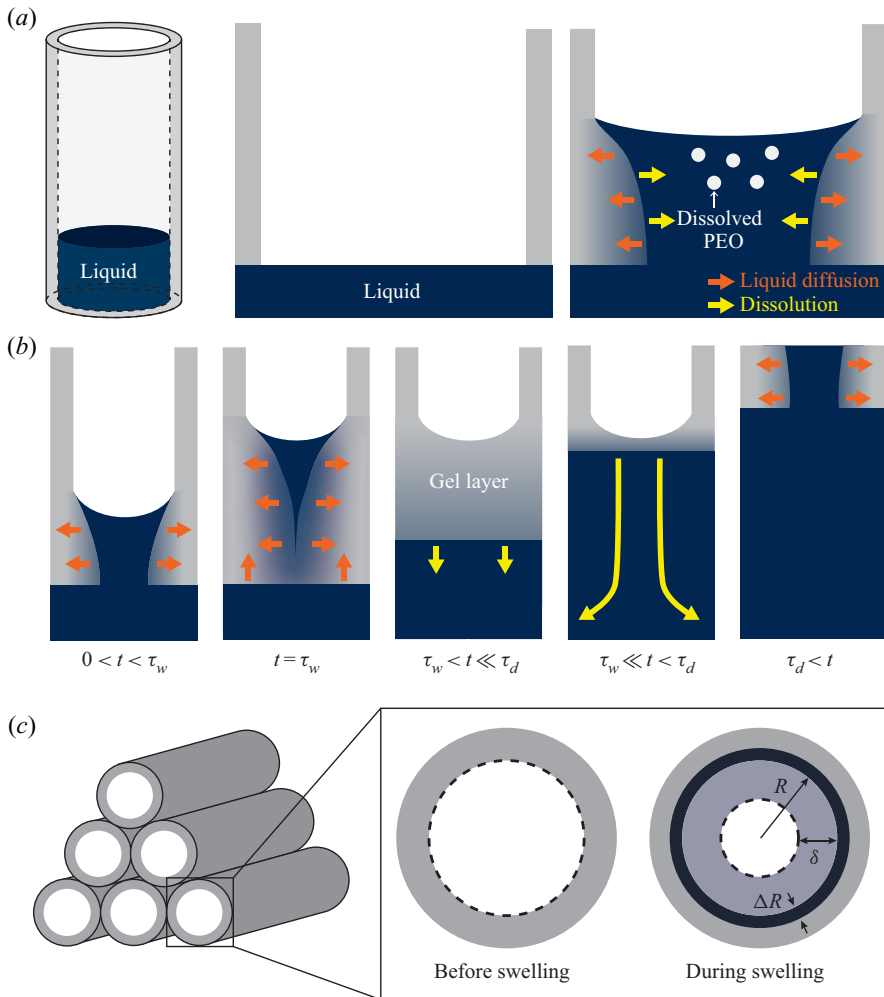
Figure 5. Schematic illustrations of solvent imbibition through a soluble capillary. (*a*) When the conduit is wide, the wicking velocity is an outcome of simultaneous interactions of capillary wicking, solvent diffusion into the wall, wall swelling and dissolution. (*b*) When the conduit is narrow, the swelling polymer blocks the conduit rapidly. The wicking speed is determined by how fast the gel layer is dissolved into the liquid. (*c*) Schematics of pore clogging process in porous media, assumed as an assemblage of cylindrical conduits of equivalent radius R, due to solvent diffusion into polymeric wall. While the solvent diffuses into an inner wall of a singe conduit by a distance ΔR, the conduit radius is reduced to $R - \delta$ due to the wall swelling as much as δ.

diffusion and consequent polymer swelling, and chemical reaction of polymer dissolution into solvent (Ha *et al.* 2018).

However, the current problem is rather directly linked to the second case of narrow conduits that are readily blocked by swelling polymer fibres. The swelling ratio of PEO due to absorption of aqueous liquids is so high (approximately 10) that voids in our porous sheets with porosity of 0.84 are clogged by the swollen polymer. Then, the wicking arises by repeating the following steps: wall swelling with capillary wicking until clogging, and reopening by polymer dissolution. Denoting the time scale of the former step as τ_w and the latter as τ_d, their sum, $\tau = \tau_w + \tau_d$, corresponds to the period of the wicking process. If λ

is the characteristic distance that a liquid travels before the conduit is clogged, the average wicking velocity is given by λ/τ. In the following, we show that the time for wicking and swelling before clogging is much shorter than the dissolution time, i.e. $\tau_d \gg \tau_w$. Then we get $\tau \approx \tau_d$ because the dissolution is the rate-determining step, which allows us to find the wicking velocity to be λ/τ_d. Therefore, we only need to consider the rate of dissolution in order to find the wicking velocity rather than considering simultaneous wicking, swelling and dissolution.

Figure 4(c) schematically illustrates the processes during soluble wicking. While liquid infiltrates into the porous sheet, the fibres surrounding pores are swollen with diffusion of the solvent (liquid). Figure 4(d) shows the swelling of PEO fibres with absorption of water, leading to buckling and contacts of initially aligned fibres. In order for the wicking to resume after this pore clogging, a sufficient amount of polymer in the gel layer should be dissolved away into the fresh liquid following the wetting front. Therefore, the liquid transport in soluble porous media is an outcome of repeated processes of capillary wicking of a short distance accompanied by pore clogging and polymer dissolution.

The soluble wicking distance L_s for a time t significantly greater than τ is then written as $L_s = \lambda t/\tau$. To estimate λ and τ, we consider the two time scales relevant to the soluble wicking.

(i) Time for wicking and swelling until clogging, τ_w. The time τ_w for liquid to wick over a distance λ owing to capillarity with negligible inertia can be given by the Washburn rule (Washburn 1921): $\lambda \sim (\sigma R \tau_w/\tilde{\mu})^{1/2}$, where $\tilde{\mu}$ is the average viscosity of liquid. As the liquid diffuses into PEO fibres, the polymer swells, so that the fluid conduit is clogged as schematically illustrated in figure 5(c). Assuming porous media as assemblages of cylindrical conduits of equivalent radius R, we consider diffusion of solvent into the inner wall of a polymeric cylindrical tube by a distance ΔR. Then the polymer swells in a way such that the conduit radius is reduced to $R - \delta$. It is known that PEO swells approximately 10 times by absorbing aqueous liquids (Abd El-Hady & Abd El-Rehim 2004), so that $\Delta R/R \sim 0.1$ when the conduit is clogged ($\delta = R$). With the characteristic swelling time scale τ_w estimated as the diffusion time scale to a distance of $\Delta R = 0.1R$, we get $\tau_w \sim (0.1R)^2/D_s$. Because the diffusion coefficients of liquids C to F into PEO fibres are of the order of $D_s \sim 10^{-9}$ m^2 s^{-1} (Vrentas & Duda 1979; Barnes *et al.* 1994), we find $\tau_w \sim 10^{-5}$ s for $R \sim 10^{-6}$ m.

(ii) Time for reopening by polymer dissolution, τ_d. The time for polymer dissolution in fresh liquid by disentanglement of loosened polymer chains is scaled as $\tau_d \sim \lambda/K_d$, where the unit wicking distance λ serves as a gel layer thickness and K_d is the rate of polymer chain detachment and diffusion into liquid. If the diffusivity of a polymer in a liquid and the radius of gyration are, respectively, denoted as D_l and r_g, K_d is scaled as $K_d \sim D_l/r_g$ (de Gennes 1979; Doi & Edwards 1988). Using the Stokes–Einstein relation (Couper & Stepto 1969), $D_l \approx k_B T/(6\pi\mu r_g)$ with k_B, T and μ respectively being the Boltzmann constant, the absolute temperature and the viscosity of fresh liquid, we estimate $\tau_d \sim 6\pi\lambda\mu r_g^2/(k_B T)$.

As the capillary wicking stops due to pore clogging by swelling, the distance λ can be obtained by substituting $\tau_w \sim (0.1R)^2/D_s$ into the foregoing Washburn rule: $\lambda \sim 0.1R[\sigma R/(\tilde{\mu}D_s)]^{1/2}$. The viscosity of wicking liquid increases exponentially with the PEO concentration, and thus we take $\tilde{\mu} \sim 1$ Pa s based on the viscosity data of an aqueous solution of PEO with molecular weight of 3×10^5 g mol^{-1} (Ebagninin, Benchabane & Bekkour 2009). Then, we find the gel layer thickness to scale as $\lambda \sim 10^{-6}$ m. This value is consistent with the thickness of a mushy layer formed at the wetting front radially emanating from a liquid source at the centre, as imaged by an inverted microscope (Nikon

Eclipse TS100) in figure 4(*e*). We obtain the estimates of the time scales $\tau_w \sim 10^{-5}$ s and $\tau_d \sim 10^{-3}$ s with a characteristic value of r_g taken to be 10^{-8} m (Werzer, Warr & Atkin 2011). Therefore, the slowest polymer dissolution is a rate-limiting step that determines the rate of liquid invasion in soluble porous sheets of PEO fibres.

We write $L_s \sim \lambda t/\tau_d$, which gives

$$L_s \sim \frac{\beta}{\mu} t, \qquad (4.2)$$

with $\beta = k_B T / r_g^2$. Figure 4(*b*) shows that the scattered data of liquid invasion distance L_s for various liquids are collapsed onto a single line when plotted according to scaling law (4.2). The slope of the line of best fit is $\alpha_s = 1.2$, leading us to write $L_s = \alpha_s \beta t/\mu$. The liquid invasion rate in soluble isotropic porous sheets is critically dependent on the viscosity but independent of surface tension of liquid, as the rate of disentanglement of polymer chains into fresh liquid determines the liquid propagation speed.

4.4. *Wicking in directionally deposited soluble sheets*

Since the lengthwise wicking in directionally deposited fibrous soluble sheets is insignificant, we plot the wicking distance in the crosswise direction L_d versus time in figure 6(*a*). The distance corresponds to the average height of spiky fronts shown in the right-hand column of figure 1(*h*). We see that the distance grows linearly with time just as for the randomly deposited sheets but at a higher rate. Since the coupled process of pore invasion–pore clogging–polymer dissolution should still arise for liquid propagation, we plot L_d versus $\beta t/\mu$ according to scaling law (4.2) in figure 6(*b*). We find the experimental data to be collapsed onto a single line with a slope $\alpha_d = 1.6$, which is 1.3 times higher than the value for the randomly deposited sheets, α_s.

To understand why the wicking of reactive liquids is fast in the crosswise direction but severely suppressed in the lengthwise direction, we schematically illustrate physical processes during crosswise and lengthwise wicking in figures 6(*c*) and 6(*d*), respectively. When the liquid front and fibre alignment are parallel (figure 6*c*), the dissolved polymer chains can be easily carried away by fresh liquid that follows the wicking front. The aligned but buckled fibres having a number of contacts with neighbours guide the flow to occur perpendicular to the fibre alignment direction without detouring, in contrast with randomly deposited, insoluble unswollen fibres that force the flow to detour in seeking easy supply path of fresh liquid. The unevenness of wet front shown in figure 1(*g*) reflects such detouring in randomly deposited substrates. The polymer dissociation is still the limiting step in liquid wicking, allowing us to write $L_d = \alpha_d \beta t/\mu$. We consider the ratio α_d/α_s a measure of randomness of fibre directionality affecting the invasion rate of liquid in soluble fibrous sheets.

When liquid attempts to flow in the lengthwise direction (figure 6*d*), the aligned fibres are continually dissolved into the diffusing solvent forming an excessively thick gel layer, which cannot meet fresh liquid to remove disentangled polymer chains. The thick gel layer blocking the lengthwise invasion is clearly observed in an SEM image obtained after a wicking test (figure 6*e*). The tip of the opening area shows a thin gel layer of the order of 10^{-6} m, facilitating the crosswise wicking to elongate the opening in the direction designated by the black arrow. Such pointed propagation of liquid while shielded by a thick gel layer in the sides appears to result in the highly spiky wet front in the right-hand column of figure 1(*h*).
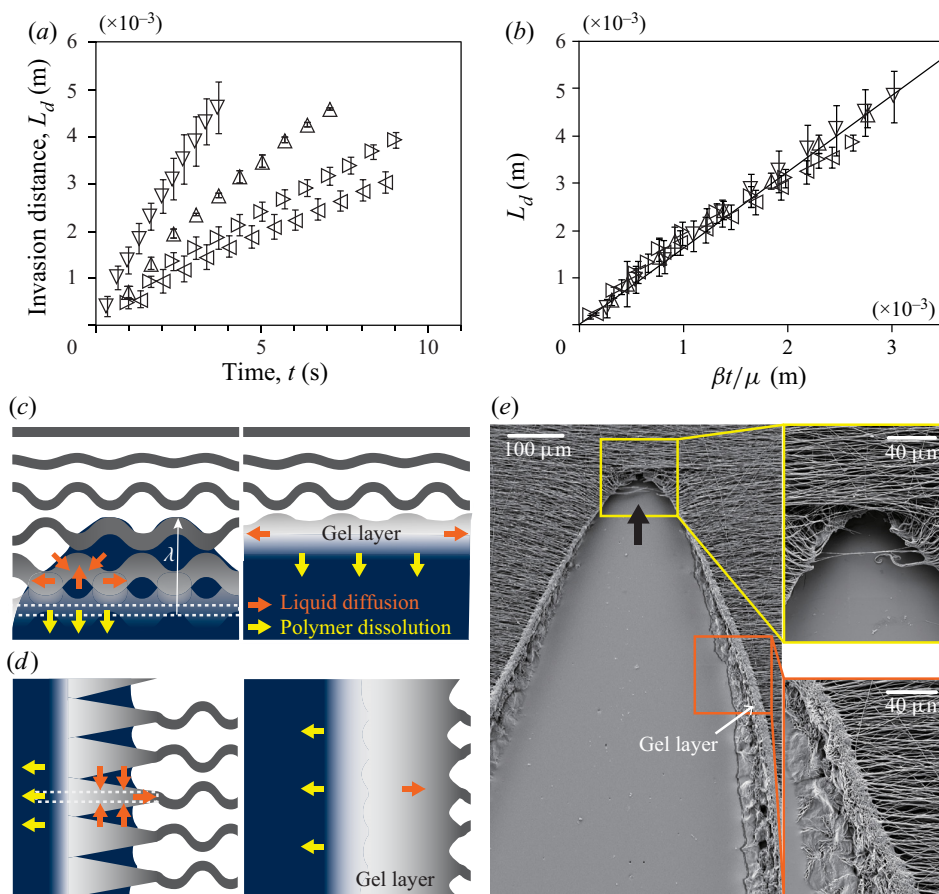
Figure 6. (*a*) The liquid invasion distance L_d of various liquids versus time in soluble porous sheets of directionally deposited PEO fibres. (*b*) Distance L_d versus $\beta t/\mu$, plotted according to scaling law (4.2). Schematics of physical processes during wicking in (*c*) the crosswise and (*d*) the lengthwise direction. (*e*) Scanning electron microscopy images of a sheet of directionally deposited fibres after wicking of water emanated from a capillary.

5. Conclusions

We have shown both experimentally and theoretically that the wicking dynamics of liquids in fibrous sheets is qualitatively different depending on whether the fibres are soluble or not. In addition, directionality of fibres has been shown to determine the preferred orientation of wicking in a solubility-dependent manner. Table 3 summarizes the findings according to the directionality and solubility of fibrous sheets. In insoluble fibrous sheets, liquids wick isotropically and diffusively ($L_r \sim t^{1/2}$) when the fibres are randomly deposited as being continuously driven by capillarity and resisted by viscosity. The diffusive dynamics still holds for the lengthwise wicking in insoluble sheets of aligned fibres, but the wicking is slower in the crosswise direction. In soluble fibrous sheets, the wicking dynamics is limited by the dissolution rate of polymer chains into liquid, so that the wicking distance grows linearly with time in randomly deposited fibrous sheets. The constant wicking rate also holds for the crosswise wicking in directionally deposited soluble fibrous sheets. But the lengthwise propagation is inhibited by excessively thick gel layers formed by continual diffusion of solvent along the aligned fibres.

| | | Directionally deposited fibrous sheet | |
	Randomly deposited fibrous sheet	Lengthwise	Crosswise
Insoluble	$L_r = 2\left[\dfrac{k_r}{\phi R}\dfrac{\sigma}{\mu}\right]^{1/2}t^{1/2}$	$L_l = 2\left[\dfrac{k_l}{\phi R}\dfrac{\sigma}{\mu}\right]^{1/2}t^{1/2}$	$L_c \sim \left(\dfrac{\sigma R^2}{\mu}t\right)^{1/3}$
Soluble	$L_s = \alpha_s \dfrac{k_B T}{r_g^2 \mu}t$	Suppressed	$L_d = \alpha_d \dfrac{k_B T}{r_g^2 \mu}t$

Table 3. Summary of the wicking dynamics depending on directionality and solubility of fibrous porous sheets. The equivalent pore radius $R = \phi R_f/(1-\phi)$.

Although capillarity-driven imbibition in insoluble fibrous media is governed by such physical properties as surface tension and viscosity of liquid and porosity and permeability of porous network, our study of soluble porous media reveals that their wicking dynamics is mainly determined by viscosity and fibre alignment. In particular, the high sensitivity of soluble wicking rates to orientation of fibre alignment opens a new pathway to accurately control dissolution behaviour of porous sheets. One can expedite dissolution of porous shells by arranging fibres perpendicular to the desired wicking direction (to induce crosswise wicking) while arranging fibres parallel to the undesired direction. It is also possible to spatially pattern the orientation of fibres so that the wicking can occur along a designated path. In practice, such delicate scheme of guided dissolution will help one to design air-trapping porous drug delivery systems (Yuasa, Takashima & Kanaya 1996; Singh & Kim 2000) capable of releasing drugs at a precisely controlled rate and direction, to encrypt messages on a soluble piece of paper (Thomas *et al.* 2009; Burgess *et al.* 2011) or to devise soft robots capable of actuation or morphing in response to surrounding chemical environments (Yang *et al.* 2018).

Declaration of interests. The authors report no conflict of interest.

Author ORCIDs.
Ⓓ Wonjung Kim https://orcid.org/0000-0002-6866-6840;
Ⓓ Ho-Young Kim https://orcid.org/0000-0002-6813-2398.

REFERENCES

ABD EL-HADY, A. & ABD EL-REHIM, H.A. 2004 Production of prednisolone by pseudomonas oleovorans cells incorporated into pvp/peo radiation crosslinked hydrogels. *Biomed. Res. Intl* **2004** (4), 219–226.

BARNES, A.C., BIEZE, T.W.N., ENDERBY, J.E. & LAYTE, J.C. 1994 Dynamics of water in the poly(ethylene oxide) hydration shell: a quasi elastic neutron-scattering study. *J. Phys. Chem.* **98**, 11527–11532.

BAVER, L.D. 1949 Retension and movement of soil moisture. In *Hydrology* (ed. O.E. Meinzer), pp. 364–384. Dover Publications.

BAYRAMLI, E. & POWELL, R.L. 1990 The normal (transverse) impregnation of liquids into axially oriented fiber bundles. *J. Colloid Interface Sci.* **138**, 346–353.

BEAR, J. 1972 *Dynamics of Fluid in Porous Media*, pp. 161–176. Elsevier.

BRIELLES, N., *et al.* 2007 Imbition and dissolution of a porous medium. *Ind. Engng Chem. Res.* **46**, 5785–5793.

BURGESS, I.B., MISHCHENKO, L., HATTON, B.D., KOLLE, M., LONCAR, M. & AIZENBERG, J. 2011 Encoding complex wettability patterns in chemically functionalized 3D photonic crystals. *J. Am. Chem. Soc.* **133**, 12430–12432.

BUCKINGHAM, E. 1914 On physically similar systems; illustrations of the use of dimensional equations. *Phys. Rev.* **4** (4), 345–376.

CAI, J. & YU, B. 2011 A discussion of the effect of tortuosity on the capillary imbibition in porous media. *Transp. Porous Med.* **89** (2), 251–263.

CARMAN, P.C. 1941 Capillary rise and capillary movement of moisture in fine sands. *Soil Sci.* **52** (1), 1–14.

COLOMBO, P., BETTINI, R., SANTI, P., DE ASCENTIIS, A. & PEPPAS, N.A. 1996 Analysis of the swelling and release mechanisms from drug delivery systems with emphasis on drug solubility and water transport. *J. Control. Release* **39**, 231–237.

CORNELL, D. & KATZ, D.L. 1953 Flow of gases through consolidated porous media. *Ind. Engng Chem.* **45** (10), 2145–2152.

COUPER, A. & STEPTO, R.F.T. 1969 Diffusion of low-molecular weight poly (ethylene oxide) in water. *T. Faraday Soc.* **65**, 2486–2496.

DACCORD, G. 1987 Chemical dissolution of a porous medium by a reactive fluid. *Phys. Rev. Lett.* **58**, 479.

DARCY, H. 1856 *Les Fontaines publiques de la ville de Dijon*. Victor Dalmont.

DOI, M. & EDWARDS, S.F. 1988 *The Theory of Polymer Dynamics*, pp. 222–236. Oxford University Press.

DUPUIT, J.È.J. 1863 *Ètudes thèoriques et pratiques sur le mouvement des eaux dans les canaux dècouverts et à travers les terrains permèables*. Dunod.

EBAGNININ, K.W., BENCHABANE, A. & BEKKOUR, K. 2009 Rheological characterization of poly (ethylene oxide) solutions of different molecular weights. *J. Colloid Interface Sci.* **336**, 360–367.

FORCHHEIMER, P. 1986 Uber die ergiebigkeit von brummen-anlagen und sickerschlitzen. *Z. Arch. Ing.-Ver. Hannover.* **32**, 539–563.

DE GENNES, P.-G. 1979 *Scaling Concepts in Polymer Physics*, pp. 165–200. Cornell University Press.

DE GENNES, P.-G., BROCHARD-WYART, F. & QUÉRÉ, D. 2004 *Capillarity and Wetting Phenomena: Drops, Bubbles, Pearls, Waves*. Springer-Verlag.

GRIFFITHS, J.C. 1952 Grain-size distribution and reservoir-rock characteristics. *Bull. Am. Assoc. Petrol. Geol.* **36** (2), 205–229.

HA, J., KIM, J., JUNG, Y., YUN, G., KIM, D.-N. & KIM, H.-Y. 2018 Poro-elasto-capillary wicking of cellulose sponges. *Sci. Adv.* **4**, eaao7051.

JACOB, C.E. 1946 Radial flow in a leaky artesian aquifer. *Trans. Am. Geophys. Un.* **27** (2), 198–208.

KOZENY, J. 1927 Uber kapillare leitung der wasser in boden. *S.-Ber. Wiener Akad., Abt.* **136**, 271–306.

KIM, J., HA, J. & KIM, H.-Y. 2017 Capillary rise of non-aqueous liquids in cellulose sponges. *J. Fluid Mech.* **818**, R2.

KIM, J., MOON, M.-W., LEE, K.-R., MAHADEVAN, L. & KIM, H.-Y. 2011 Hydrodynamics of writing with ink. *Phys. Rev. Lett.* **107**, 264501.

KIM, S.J., CHOI, J.W., MOON, M.W., LEE, K.R., CHANG, Y.S., LEE, D.Y. & KIM, H.-Y. 2015 Wicking and flooding of liquids on vertical porous sheets. *Phys. Fluids* **27**, 032105.

LANDERYOU, M., EAMES, I. & COTTENDEN, A. 2005 Infiltration into inclined fibrous sheets. *J. Fluid Mech.* **529**, 173–193.

MAO, N. & RUSSELL, S.J. 2008 Capillary pressure and liquid wicking in three-dimensional nonwoven materials. *J. Appl. Phys.* **104**, 034911.

NELSON, W.R. & BAVER, L.D. 1940 Movement of water through soils in relation to the nature of the pores. *Proc. Soil. Sci. Soc. Am.* **5**, 60–76.

PURCELL, W.R. 1949 Capillary pressures-their measurement using mercury and the calculation of permeability therefrom. *J. Petrol. Tech.* **1** (02), 39–48.

RAUX, R.S., COCKENPOT, H., RAMAIOLI, M., QUÉRÉ, D. & CLANET, C. 2013 Wicking in a powder. *Langmuir* **29**, 3636–3644.

RODRIGUEZ, E., GIACOMELLI, F. & VAZQUEZ, A. 2004 Permeability-porosity relationship in rtm for different fiberglass and natural reinforcements. *J. Compos. Mater.* **38**, 259–268.

ROSE, W. & WITHERSPOON, P.A. 1956 *Studies of Waterflood Performance*. Division of the Ill. State Geol. Survey.

SCHEIDEGGER, A.E. 1960 *The Physics of Flow Through Porous Media*, pp. 124–151. University of Toronto Press.

SHIN, B., HA, J., LEE, M., PARK, K., PARK, G.H., CHOI, T.H., CHO, K.-J. & KIM, H.-Y. 2018 Hygrobot: a self-locomotive ratcheted actuator powered by environmental humidity. *Sci. Robot.* **3**, eaar2629.

SINGH, B.N. & KIM, K.H. 2000 Floating drug delivery systems: an approach to oral controlled drug delivery via gastric retention. *J. Control. Release* **63**, 235–259.

SZYMCZAK, P. & LADD, A.J. 2011 Instabilities in the dissolution of a porous matrix. *Geophys. Res. Lett.* **38**, L07403.

THOMAS, S.W., CHIECHI, R.C., LAFRATTA, C.N., WEBB, M.R., LEE, A., WILEY, B.J., ZAKIN, M.R., WALT, D.R. & WHITESIDES, G.M. 2009 Infochemistry and infofuses for the chemical storage and transmission of coded information. *Proc. Natl Acad. Sci. USA* **106**, 9147–9150.

TWIST, J.N. & ZATZ, J.L. 1988 Membrane–solvent–solute interaction in a model permeation system. *J. Pharm. Sci.* **77**, 536–540.

VRENTAS, J.S. & DUDA, J.L. 1979 Molecular diffusion in polymer solutions. *AIChE J.* **25**, 1–24.

WASHBURN, E.W. 1921 The dynamics of capillary flow. *Phys. Rev.* **17**, 273.

WERZER, O., WARR, G.G. & ATKIN, R. 2011 Compact poly (ethylene oxide) structures adsorbed at the ethylammonium nitrate-silica interface. *Langmuir* **27**, 3541–3549.

XIA, D. & BRUECK, S.R.J. 2008 Strongly anisotropic wetting on one-dimensional nanopatterned surfaces. *Nano Lett.* **8**, 2819–2824.

YANG, G.-Z., *et al.* 2018 The grand challenges of science robotics. *Sci. Robot.* **3**, eaar7650.

YOON, J., CAI, S., SUO, Z. & HAYWARD, R.C. 2010 Poroelastic swelling kinetics of thin hydrogel layers: comparison of theory and experiment. *Soft Matt.* **6**, 6004–6012.

YUASA, H., TAKASHIMA, Y. & KANAYA, Y. 1996 Studies on the development of intragastric floating and sustained release preparation. I. Application of calcium silicate as a floating carrier. *Chem. Pharm. Bull.* **44**, 1361–1366.